Title

Inhibited Methanogenesis in the Rumen of Cattle: Microbial Metabolism in Response to Supplemental 3-Nitrooxypropanol and Nitrate

Authors

van Lingen, Henk J

Fadel, James G

Yáñez-Ruiz, David R

et al.

Publication Date

2021

DOI

10.3389/fmicb.2021.705613

frontiers in Microbiology

ORIGINAL RESEARCH
published: 27 July 2021
doi: 10.3389/fmicb.2021.705613

Inhibited Methanogenesis in the Rumen of Cattle: Microbial Metabolism in Response to Supplemental 3-Nitrooxypropanol and Nitrate

Henk J. van Lingen[1*†], *James G. Fadel*[1], *David R. Yáñez-Ruiz*[2], *Maik Kindermann*[3] *and Ermias Kebreab*[1]

[1] Department of Animal Science, University of California, Davis, Davis, CA, United States, [2] Estación Experimental del Zaidín (CSIC), Granada, Spain, [3] Research and Development, DSM Nutritional Products, Basel, Switzerland

OPEN ACCESS

Edited by:
Shyam Sundar Paul, Directorate of Poultry Research (DPR), ICAR, India

Reviewed by:
Xuezhao Sun, Jilin Agricultural Science and Technology University, China
Kevin Thomas Finneran, Clemson University, United States

***Correspondence:**
Henk J. van Lingen
henk.vanlingen@wur.nl

†Present address:
Henk J. van Lingen, Laboratory of Systems and Synthetic Biology, Wageningen University & Research, Wageningen, Netherlands

Specialty section:
This article was submitted to Systems Microbiology, a section of the journal Frontiers in Microbiology

Received: *05 May 2021*
Accepted: *28 June 2021*
Published: *27 July 2021*

Citation:
van Lingen HJ, Fadel JG, Yáñez-Ruiz DR, Kindermann M and Kebreab E (2021) Inhibited Methanogenesis in the Rumen of Cattle: Microbial Metabolism in Response to Supplemental 3-Nitrooxypropanol and Nitrate. Front. Microbiol. 12:705613. doi: 10.3389/fmicb.2021.705613

3-Nitrooxypropanol (3-NOP) supplementation to cattle diets mitigates enteric CH_4 emissions and may also be economically beneficial at farm level. However, the wider rumen metabolic response to methanogenic inhibition by 3-NOP and the NO_2^- intermediary metabolite requires further exploration. Furthermore, NO_3^- supplementation potently decreases CH_4 emissions from cattle. The reduction of NO_3^- utilizes H_2 and yields NO_2^-, the latter of which may also inhibit rumen methanogens, although a different mode of action than for 3-NOP and its NO_2^- derivative was hypothesized. Our objective was to explore potential responses of the fermentative and methanogenic metabolism in the rumen to 3-NOP, NO_3^- and their metabolic derivatives using a dynamic mechanistic modeling approach. An extant mechanistic rumen fermentation model with state variables for carbohydrate substrates, bacteria and protozoa, gaseous and dissolved fermentation end products and methanogens was extended with a state variable of either 3-NOP or NO_3^-. Both new models were further extended with a NO_2^- state variable, with NO_2^- exerting methanogenic inhibition, although the modes of action of 3-NOP-derived and NO_3^--derived NO_2^- are different. Feed composition and intake rate (twice daily feeding regime), and supplement inclusion were used as model inputs. Model parameters were estimated to experimental data collected from the literature. The extended 3-NOP and NO_3^- models both predicted a marked peak in H_2 emission shortly after feeding, the magnitude of which increased with higher doses of supplement inclusion. The H_2 emission rate appeared positively related to decreased acetate proportions and increased propionate and butyrate proportions. A decreased CH_4 emission rate was associated with 3-NOP and NO_3^- supplementation. Omission of the NO_2^- state variable from the 3-NOP model did not change the overall dynamics of H_2 and CH_4 emission and other metabolites. However, omitting the NO_2^- state variable from the NO_3^- model did substantially change the dynamics of H_2 and CH_4 emissions indicated by a decrease in both H_2 and CH_4 emission after feeding. Simulations do not

point to a strong relationship between methanogenic inhibition and the rate of NO_3^- and NO_2^- formation upon 3-NOP supplementation, whereas the metabolic response to NO_3^- supplementation may largely depend on methanogenic inhibition by NO_2^-.

Keywords: 3-NOP, nitrite, cattle, feed supplement, bacteria, archaea, methane

1. INTRODUCTION

Animal agriculture emits about 7.1 gigatonnes of CO_2 equivalents of greenhouse gases per year, which represents approximately 14.5% of total global anthropogenic greenhouse gas emissions in 2005 (Gerber et al., 2013). Dairy and beef cattle emitted 4.6 gigatonnes CO_2 equivalents, of which CH_4 from enteric fermentation contributed about 45%. To decrease the latter enteric source of greenhouse gas emission, various dietary supplements with a potential inhibiting effect on ruminal methanogenesis have been tested. 3-nitrooxypropanol (3-NOP) is one of the most effective dietary supplements that was tested for cattle (e.g., Hristov et al., 2015), and may also be economically beneficial (Alvarez-Hess et al., 2019). The mode of action of 3-NOP was elucidated to be the inhibition of methyl co-enzyme-M reductase (MCR), with clear indications that NO_2^- can be metabolized from 3-NOP and inhibit methanogenesis by blocking MCR activity as well (Duin et al., 2016). However, the wider effects of 3-NOP and NO_2^- on methanogenic archaea in the rumen and the implications for the dynamics of ruminal metabolites require a more thorough exploration.

Nitrate is another dietary supplement (commonly in the form of a calcium salt, sometimes a sodium or potassium salt) that has been observed to decrease enteric CH_4 from cattle substantially and persistently (Van Zijderveld et al., 2011), although there seem no on-farm economical benefits (Alvarez-Hess et al., 2019). Nitrate is primarily reduced to NH_3 by ruminal bacteria, which may result in the utilization of four equivalents of H_2 per equivalent of NO_3^-. This reduction reaction causes less H_2 available for CH_4 production by the methanogens. However, NO_3^- supplementation to dairy cattle diets was reported to increase H_2 emissions (Olijhoek et al., 2016). The latter increase was explained by NO_3^- being reduced to NO_2^-, with NO_2^- inhibiting the methanogenic metabolism (Latham et al., 2016). Therefore, the presence of NO_2^- as an intermediate in the reduction of NO_3^- to NH_3 may contribute to the CH_4 suppressing effect of NO_3^- supplementation to cattle diets as well.

Various ruminal bacteria possess and express genes that result in the employment of periplasmic NO_3^- and NO_2^- reductases (Kern and Simon, 2009; Yang et al., 2016). The methanogens that reside in the rumen, however, were not observed to transcribe genes that encode for NO_3^- and NO_2^- reductases (Greening et al., 2019). Lack of these reductases may suggest that the conversion of 3-NOP into NO_2^- inside methanogenic cells proceeds spontaneously or is catalyzed by different enzymes, which aligns with the formation of NO_3^- and NO_2^- upon the inactivation of the MCR enzyme (Duin et al., 2016). Although 3-NOP is transported across the methanogenic cell membrane, no evidence for NO_2^- transportation across the methanogenic cell membrane is known to the authors. If NO_2^- is transported across the methanogenic cell membrane, the NO_2^- derived from NO_3^- may even inhibit CH_4 production completely by blocking MCR at the commonly used dietary inclusion rates of NO_3^-, which is not commonly observed. On a molar basis, the relatively low inclusion rates of 3-NOP compared to NO_3^- will likely result in lower NO_2^- production. Therefore, the mechanisms by which NO_2^- derived from NO_3^- and 3-NOP act on archaea appear different, with 3-NOP derived NO_2^- exerting its methanogenic inhibition inside the cell and NO_3^- derived NO_2^- potentially exerting methanogenic inhibition outside the cell.

Besides metabolic conversions and their enzyme kinetic implications, several studies suggested the inhibiting effect of 3-NOP and NO_3^- on ruminal methanogenesis to be partly thermodynamically controlled (Van Zijderveld et al., 2011; Dijkstra et al., 2018). Both 3-NOP and NO_3^- were found to increase H_2 emission, suggesting thermodynamic inhibition of NADH oxidation in fermentative microbes in the rumen (Van Lingen et al., 2016). This thermodynamic inhibition results in a shift from acetate to more propionate production, which decreases the yield of H_2 and next the yield of CH_4. The objective of this study is to explore putative mechanisms of methanogenic inhibition by 3-NOP and NO_3^- and their implications for the dynamics of microbial fermentation in the bovine rumen using dynamic mechanistic modeling approaches. For this objective, an existing dynamic mechanistic model of microbial substrate degradation that incorporated various metabolic pathways (Van Lingen et al., 2019) is extended with putative kinetic downregulation mechanisms of methanogenesis by 3-NOP, NO_3^- and their derivatives. These newly developed modeling approaches also enable the evaluation of the thermodynamic control of H_2 partial pressure (p_{H_2}) on volatile fatty acid (VFA) fermentation pathways via the NAD^+ to NADH ratio in fermentative microbes upon the supplementation of feed with 3-NOP and NO_3^-.

2. MODEL DESCRIPTION

An extant dynamic mechanistic rumen fermentation model with state variables for ruminal carbohydrate substrates, bacteria and protozoa, gaseous and dissolved fermentation end products and methanogens (Van Lingen et al., 2019) was extended with a representation of either the 3-NOP or NO_3^- metabolism. The extant model represents the hydrolysis of carbohydrate polymers (viz., degradable fiber, degradable starch and sugars) into hexose, the thermodynamic control of p_{H_2} on volatile fatty acid (VFA) fermentation pathways via the NAD^+ to NADH ratio in fermentative microbes,

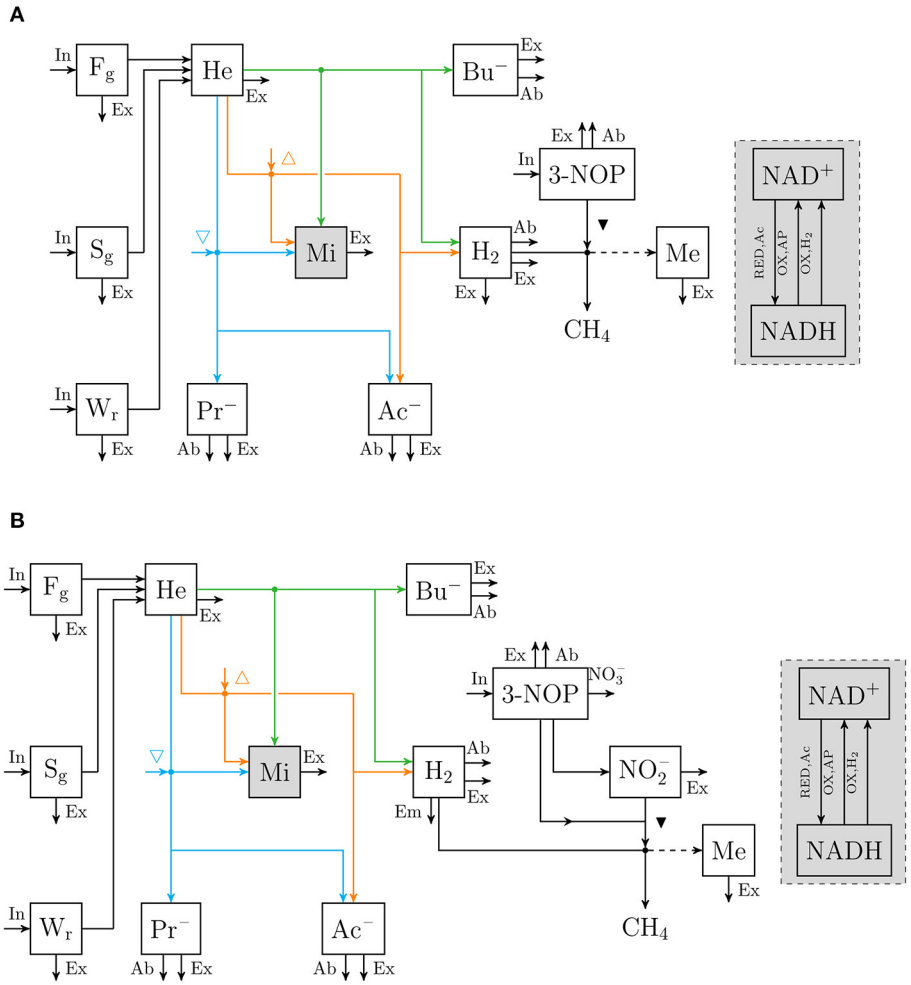

FIGURE 1 | Flow chart that conceptually represent **(A)** the rumen 3-nitrooxypropanol simple model, and **(B)** the rumen 3-nitrooxypropanol+nitrite model. Boxes enclosed by solid lines represent state variables (with F_g for degradable fiber [g], S_g for degradable starch [g], W_r for soluble carbohydrates [g], He for hexose [mol], Mi for fermentative microbes [g], Ac^- for acetate [mol], Pr^- for propionate [mol], Bu^- for butyrate [mol], H_2 for hydrogen [mol], 3-NOP for 3-nitrooxypropanol [mol], NO_2^- for nitrite [mol], Me for methanogens [g]. The sum of NAD^+ and NADH [mol] is a fraction of Mi and a gray fill is used to visualize this), arrows represent fluxes with the dashed arrow indicating H_2 is not incorporated but its conversion to CH_4 is required for growth (with In for dietary input, Ex for fractional exit from the rumen to the lower tract, Ab fractional absorption, Em for fractional emission, NO_3^- for nitrate production, RED, Ac for NAD^+ reduction associated with hexose converted into 2 Ac, {OX,AP} for NADH oxidation associated with hexose converted into $\frac{2}{3}$ Ac^- + $\frac{4}{3}$ Pr^-, and {OX,H_2} for hydrogenase catalyzed NADH oxidation; △ and ▽ indicate that at increased NAD^+ to NADH ratio the microbial conversion is promoted and inhibited, respectively; ▼ indicates inhibition of methanogenesis; fluxes may be unique per state variable and are further specified in Van Lingen et al. (2019), dots indicate microbial conversions.

and hydrogenotrophic methanogenesis in the bovine rumen. Four different extensions of the original model were made. These model extensions comprised a representation of 3-NOP and NO_3^- and with and without NO_2^-, which is derived from both 3-NOP and NO_3^-, respectively. The four extended models are diagrammatically represented in **Figures 1**, **2**, while a schematic overview of physiological characteristics incorporated per model is provided in **Table 1A**. Mathematical notation of influxes and outfluxes of model state variables is $P_{i;j,m}$ and $U_{i;j,m;n}$, respectively, where the subscript represents the uptake or production of i by j-to-m transaction (generating n). To illustrate this, $P_{3NOP;In,3NOP}$ represents the increase in 3-NOP as a result of the inflow of 3-NOP. Concentrations of i are computed as:

$$C_i = \frac{Q_i}{V_{Fl}} \tag{1}$$

for $i = \{H_2, 3\text{-NOP}, NO_3^-, NO_2^-\}$ and V_{Fl} being the rumen fluid volume. State variables are expressed in [g] or [mol], with the corresponding fluxes and concentrations expressed in [mol·h^{-1}] or [g·h^{-1}], and [mol·L^{-1}] or [g·L^{-1}], respectively. Abbreviations and general notation are available in **Table 2**. Parameters specific for the new models are provided in **Table 3**.

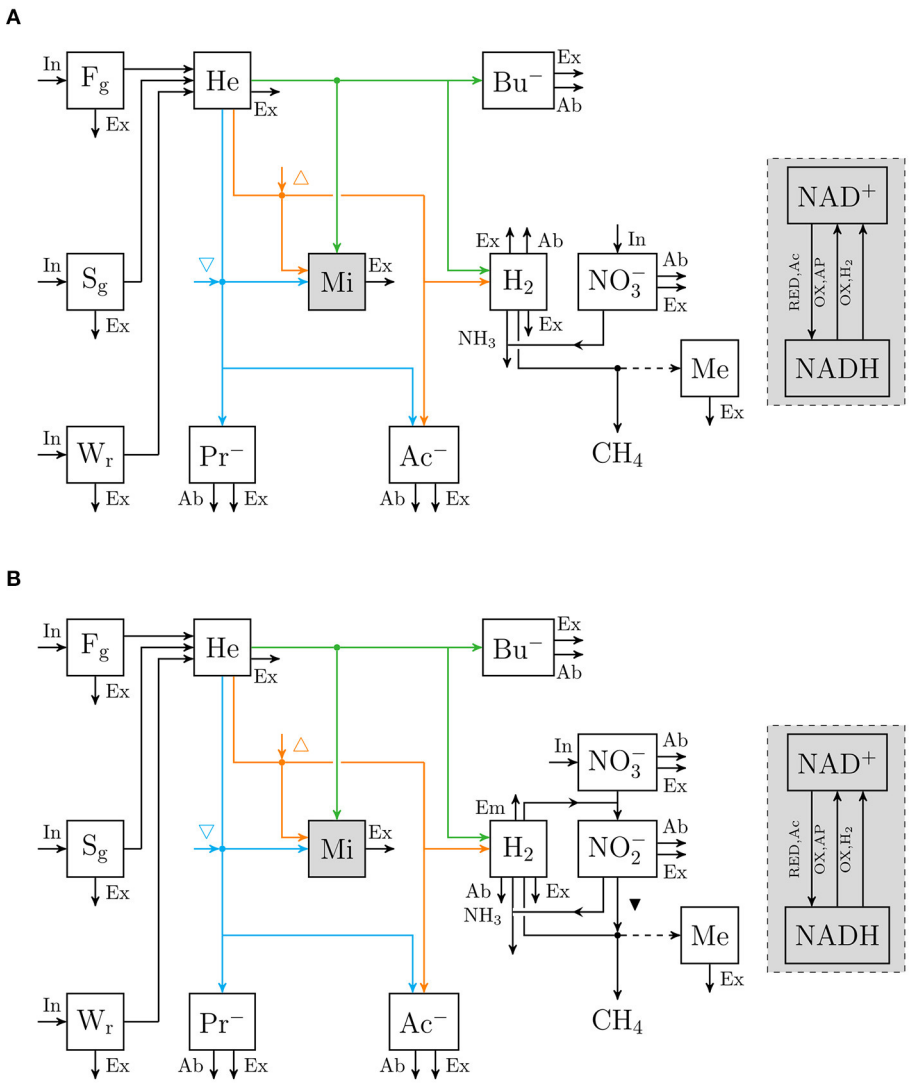

FIGURE 2 | Flow chart that conceptually represent **(A)** the rumen nitrate simple model, and **(B)** the rumen nitrate+nitrite model. Boxes enclosed by solid lines represent state variables (with NO_3^- for nitrate [mol] and NO_2^- for nitrite [mol]; ▼ indicates inhibition of methanogenesis; other abbreviations are described in **Figure 1**), dots indicate microbial conversions.

2.1. Mathematical Representation of Model Extentions

2.1.1. 3-NOP Simple Model

3-nitrooxypropanol state variable, Q_{3NOP} [mol]. The Q_{3NOP} state variable receives input from 3-NOP contents in the feed that was supplemented:

$$P_{3NOP;In,3NOP} = D_{DM}(t) \cdot c_{3NOP} \quad (2)$$

with $D_{DM}(t)$ the dry matter intake rate in time [kg·h^{-1}] and c_{3NOP} the 3-NOP content of the feed [mol·kg^{-1}]. 3-NOP can easily diffuse through membranes (Duin et al., 2016) and was assumed to be absorbed across the rumen wall:

$$U_{3NOP;3NOP,Ab} = k_{3NOP,Ab} \cdot Q_{3NOP}, \quad (3)$$

with $k_{3NOP,Ab}$ the fractional absorption rate of 3-NOP (value and units in **Table 3**). Finally 3-NOP was assumed to flow out to the lower tract with the fluid fraction, which was represented as:

$$U_{3NOP;3NOP,Ex} = k_{Fl,Ex} \cdot Q_{3NOP} \quad (4)$$

with $k_{Fl,Ex}$ the fractional outflow rate of the fluid fraction [h^{-1}] as in Van Lingen et al. (2019). The differential equation of the Q_{3NOP} state variable is given by:

$$\frac{dQ_{3NOP}}{dt} = P_{3NOP;In,3NOP} - U_{3NOP;3NOP,Ab} - U_{3NOP;3NOP,Ex} \quad (5)$$

Hydrogen state variable, Q_{H_2} [mol]. As described by Van Lingen et al. (2019), inputs to the Q_{H_2} state variable are

TABLE 1 | Overview of **(A)** physiological characteristics regarding methanogenic inhibition and H_2 sinks incorporated in 3-NOP, 3-NOP+nitrite, nitrate and nitrate+nitrite models, along with **(B)** the physiological response of various output variables to dietary inclusion of 3-NOP or NO_3^-.

	3-NOP	3-NOP+nitrite	Nitrate	Nitrate+nitrite
(A) Physiological characteristic				
Methanogenic inhibition by 3-NOP (MCR[a])	✓	✓		
3-NOP to NO_3^- + NO_2^- (MCR[a])		✓		
Methanogenic inhibition by NO_2^- (MCR[a])		✓		
NO_3^- to NH_3 (H_2 sink)			✓	
NO_3^- to NO_2^- (H_2 sink)				✓
NO_2^- to NH_3 (H_2 sink)				✓
Methanogenic inhibition by NO_2^- (hypothesized[b])				✓
(B) Response to supplemented 3-NOP or NO_3^-				
H_2 emission rate and p_{H_2}	↑	↑	↓	↑
CH_4 emission rate	↓	↓	↓	↓
Inhibition on NADH oxidation	↑	↑	↓	↑
Acetate proportion	↓	↓	-	↓
Propionate proportion	↑	↑	-	↑
Butyrate proportion	↑	↑	-	↑

Check-marks indicate if a physiological characteristic was incorporated. Upward and downward arrows indicate up-regulation and down-regulation of the metabolism, respectively, a dash indicates a response was negligibly small.
[a]Reflects inhibition of archaeal methyl co-enzyme-M reductase. [b]Mode of action of methanogenic inhibition by NO_3^- derived NO_2^- remains to be fully determined. See also sections 2.1.4 and 4.2.

TABLE 2 | Abbreviations used in mathematical expressions in the model.

Symbol	Entity	Symbol	Entity
Ab	Absorption	La	Lactate
Ac	Acetate	Me	Methanogens
AP	Acetate + propionate	Mi	Fermentative microbes
Bu	Butyrate	P_g	Degradable protein
DM	Dry matter	Pr	Propionate
Em	Emission (from the rumen)	P_s	Soluble protein
Ex	Exit to lower tract	S_g	Degradable starch
F_g	Degradable fiber	So	Solid
Fl	Fluid	S_r	Soluble starch
He	Hexose	W_r	Water soluble carbohydrates
In	Intake		

TABLE 3 | Preliminary parameter values used in the 3-NOP, 3-NOP+NO_2^-, NO_3^-, and NO_3^-+NO_2^- models.

Variable	Units	3-NOP	3-NOP+NO_2^-	NO_3^-	NO_3^-+NO_2^-
$k_{NO_x^-,Ab}$	h^{-1}	–	–	0.30	0.30
$k_{3NOP,Ab}$	h^{-1}	0.30	0.30	–	–
$k_{NO_3^-,NH_3}$	$mol^{-1}g^{-1}h^{-1}$			6.99	
$k_{NO_3^-,NO_2^-}$	$mol^{-1}g^{-1}h^{-1}$				1.5
$k_{NO_2^-,NH_3}$	$mol^{-1}g^{-1}h^{-1}$				0.113
k_{3NOP,NO_3^-}	$g^{-1}h^{-1}$		1.55		
k_{3NOP,NO_2^-}	$g^{-1}h^{-1}$		0.44		
$J_{NO_2^-;H_2,Me}$	M				1.17e-3
$J_{MCR,H_2,Me}$	M	1.93e-5	2.10e-5		

H_2 influxes associated with acetate and butyrate production ($P_{H_2;He,Ac}$ and $P_{H_2;He,Bu}$), whereas outputs that are copied to the present model are emission, outflow with rumen fluid and absorption of H_2 ($U_{H_2;H_2,Em}$, $U_{H_2;H_2,Ex}$, and $U_{H_2;H_2,Ab}$, respectively). In the present model, the outflux that represents H_2 utilization for 3-NOP inhibited methanogenic growth is given by:

$$U_{H_2;H_2,CH_4} = \frac{v_{H_2,CH_4} \cdot Q_{Me}}{1 + \frac{M_{H_2;H_2,CH_4}}{C_{H_2}} + \frac{C_{3NOP}}{J_{MCR;H_2,CH_4}}} \quad (6)$$

where v_{H_2,CH_4} denotes the maximum utilization rate of H_2 by archaea [$mol \cdot g^{-1}h^{-1}$; from Van Lingen et al. (2019)], Q_{Me} the methanogen state variable, $M_{H_2;H_2,CH_4}$ the saturation constant for H_2 utilization for methangenesis [M; from Van Lingen et al. (2019)], C_{H_2} the dissolved H_2 concentration, C_{3NOP} the 3-NOP concentration and $J_{MCR;H_2,CH_4}$ the inhibition constant of 3-NOP associated with hydrogenotrophic methanogenesis (**Table 3**). The differential equation is given by:

$$\frac{dQ_{H_2}}{dt} = P_{H_2;He,Ac} - P_{H_2;He,Bu} - U_{H_2;H_2,Ex} - U_{H_2;H_2,Em} - U_{H_2;H_2,Ab} - U_{H_2;H_2,CH_4}. \quad (7)$$

2.1.2. 3-Nitrooxypropanol+Nitrite Model

According to Duin et al. (2016), 3-NOP is broken down to NO_3^- and NO_2^- along with the formation of 1,3-propanediol. These conversions may take place in the archaeal cytosol that contribute to the presence NO_2^- that also inhibits MCR. For evaluating the implications of these metabolic steps, an extended 3-NOP model was developed that also comprised a $Q_{NO_2^-}$ state variable.

3-nitrooxypropanol state variable, Q_{3NOP} [mol]. In addition to the inputs and outputs described for the simple 3-NOP model, the conversion of 3-NOP into NO_3^- and NO_2^- is described as output from the Q_{3NOP} state variable in the present model by:

$$U_{3NOP;3NOP,NO_3^-} = k_{3NOP,NO_3^-} \cdot Q_{Me} \cdot Q_{3NOP} \quad (8)$$

and

$$U_{3NOP;3NOP,NO_2^-} = k_{3NOP,NO_2^-} \cdot Q_{Me} \cdot Q_{3NOP} \quad (9)$$

swith k_{3NOP,NO_3^-} and k_{3NOP,NO_2^-} the fractional rate constants for the conversion of 3-NOP reduction to NO_3^- and NO_2^- (**Table 3**) and the reduction flow rate is assumed to be also dependent on the methanogenic biomass. It was assumed that NO_3^- and NO_2^- is not transported across the methanogenic cell membrane and no other outputs were represented. This resulted in the differential equation of the Q_{3NOP} state variable in the 3-NOP extended model given by:

$$\frac{dQ_{3NOP}}{dt} = P_{3NOP;In,3NOP} - U_{3NOP;3NOP,NO_3^-} - U_{3NOP;3NOP,NO_2^-} - U_{3NOP;3NOP,Ab} - U_{3NOP;3NOP,Ex} \quad (10)$$

Nitrite state variable, $Q_{NO_2^-}$ [mol]. Input to the $Q_{NO_2^-}$ state variable was NO_2^- production from 3-NOP reduction:

$$P_{NO_2^-;3NOP,NO_2^-} = U_{3NOP;3NOP,NO_2^-} \quad (11)$$

and outflow from the rumen to the lower tract is with the methanogens as in Van Lingen et al. (2019):

$$U_{NO_2^-;NO_2^-,Ex} = 0.4 \cdot (k_{Fl,Ex} + k_{So,Ex}) \cdot Q_{NO_2^-} \quad (12)$$

with $k_{So,Ex}$ the fractional outflow rate of the solid material as in Van Lingen et al. (2019). The differential equation is given by:

$$\frac{dQ_{NO_2^-}}{dt} = P_{NO_2^-;3NOP,NO_2^-} - U_{NO_2^-;NO_2^-,Ex} \quad (13)$$

Hydrogen state variable, Q_{H_2} [mol]. Compared with the 3-NOP simple model, the outflux that represents H_2 utilization for methanogenesis in the 3-NOP+nitrite model also accounts for inhibition of methanogenic growth by NO_2^-, which is given by:

$$U_{H_2;H_2,CH_4} = \frac{\nu_{H_2,CH_4} \cdot Q_{Me}}{1 + \frac{M_{H_2;H_2,CH_4}}{C_{H_2}} + \frac{C_{3NOP} + C_{NO_2^-}}{J_{MCR;H_2,CH_4}}} \quad (14)$$

where $J_{MCR;H_2,CH_4}$ denotes the inhibition constant with respect to the aggregated concentrations of 3-NOP and NO_2^- (**Table 3**).

The differential equation for the 3-NOP+NO_2^- extended model is given by:

$$\frac{dQ_{H_2}}{dt} = P_{H_2;He,Ac} - P_{H_2;He,Bu} - U_{H_2;H_2,Ex} - U_{H_2;H_2,Em} - U_{H_2;H_2,Ab} - U_{H_2;H_2,CH_4}. \quad (15)$$

2.1.3. Nitrate Simple Model

The key mechanism for the decrease in CH_4 production after supplementing NO_3^- is generally considered the utilization of H_2 (Yang et al., 2016). The model was extended with only a NO_3^- state variable for evaluating the significance of this mechanism.

Nitrate state variable, $Q_{NO_3^-}$ [mol]. The $Q_{NO_3^-}$ state variable receives input from NO_3^- contents in the feed that was supplemented:

$$P_{NO_3^-;In,NO_3^-} = D_{DM}(t) \cdot c_{NO_3^-} \quad (16)$$

with $c_{NO_3^-}$ the NO_3^- content of the feed [mol·kg^{-1}]. Output comprised the reduction of NO_3^- to NH_3 in the periplasm of fermentative microbes (Kern and Simon, 2009):

$$U_{NO_3^-;NO_3^-,NH_3} = k_{NO_3^-,NH_3} \cdot Q_{Mi} \cdot Q_{NO_3^-} \cdot Q_{H_2} \quad (17)$$

with $k_{NO_3^-,NH_3}$ the rate constant for NO_3^- reduction to NH_3 (**Table 3**). The absorption of NO_3^- across the rumen wall was represented as:

$$U_{NO_3^-;NO_3^-,Ab} = k_{NO_x^-,Ab} \cdot Q_{NO_3^-} \quad (18)$$

with $k_{NO_x^-,Ab}$ the fractional absorption rate for NO_3^- absorption (**Table 3**). NO_3^- was assumed to flow out with the fluid fraction from the rumen to the lower tract:

$$U_{NO_3^-;NO_3^-,Ex} = k_{Fl,Ex} \cdot Q_{NO_3^-} \quad (19)$$

The differential equation is given by:

$$\frac{dQ_{NO_3^-}}{dt} = P_{NO_3^-;In,NO_3^-} - U_{NO_3^-;NO_3^-,Ab} - U_{NO_3^-;NO_3^-,Ex} - U_{NO_3^-;NO_3^-,NH_3} \quad (20)$$

Hydrogen state variable, Q_{H_2} [mol]. Influxes and outfluxes that were taken from Van Lingen et al. (2019) were the same as for the 3-NOP model. In the NO_3^- model, output represented H_2 utilization for NO_3^- reduction to NH_3 while applying a 4:1 stoichiometric ratio:

$$U_{H_2;NO_3^-,NH_3} = 4 \cdot U_{NO_3^-;NO_3^-,NH_3} \quad (21)$$

The flux that represented H_2 utilization for methanogenic growth was copied from the Van Lingen et al. (2019) model:

$$U_{H_2;H_2,CH_4} = \frac{\nu_{H_2,CH_4} \cdot Q_{Me}}{1 + \frac{M_{H_2;H_2,CH_4}}{C_{H_2}}} \quad (22)$$

The differential equation is given by:

$$\frac{dQ_{H_2}}{dt} = P_{H_2;He,Ac} + P_{H_2;He,Bu} - U_{H_2;H_2,Me} - U_{H_2;NO_3^-,NH_3} - U_{H_2;H_2,Ab} - U_{H_2;H_2,Em} - U_{H_2;H_2,Ex.} \quad (23)$$

2.1.4. Nitrate+Nitrite Model

For evaluating the significance of the NO_2^- intermediary metabolite on the metabolism, an extended NO_3^- model was developed for which a $Q_{NO_2^-}$ state variable was also included.

Nitrate state variable, $Q_{NO_3^-}$ [mol]. The $U_{NO_3^-;NO_3^-,NH_3}$ of the $Q_{NO_3^-}$ state variable in the simple model was broken up in two parts in the extended model. The first part resulted in output that comprised the reduction of NO_3^- to NO_2^- in the periplasm of fermentative microbes (Kern and Simon, 2009):

$$U_{NO_3^-;NO_3^-,NO_2^-} = k_{NO_3^-,NO_2^-} \cdot Q_{Mi} \cdot Q_{NO_3^-} \cdot Q_{H_2} \quad (24)$$

with $k_{NO_3^-,NO_2^-}$ the rate constant for NO_3^- reduction to NO_2^- by fermentative microbes (**Table 3**). Inflow, absorption across the rumen wall and outflow to the lower gastrointestinal tract were represented identical to the nitrate simple model, which resulted in a differential equation given by:

$$\frac{dQ_{NO_3^-}}{dt} = P_{NO_3^-;In,NO_3^-} - U_{NO_3^-;NO_3^-,Ab} - U_{NO_3^-;NO_3^-,Ex} - U_{NO_3^-;NO_3^-,NO_2^-} \quad (25)$$

Nitrite state variable, $Q_{NO_2^-}$ [mol]. Input to the $Q_{NO_2^-}$ state variable was NO_2^- production from NO_3^- reduction:

$$P_{NO_2^-;NO_3^-,NO_2^-} = U_{NO_3^-;NO_3^-,NO_2^-}, \quad (26)$$

whereas output from this state variable comprised absorption of NO_2^- across the rumen wall:

$$U_{NO_2^-;NO_2^-,Ab} = k_{NO_x^-,Ab} \cdot Q_{NO_2^-} \quad (27)$$

with $k_{NO_x^-,Ab}$ the fractional absorption rate for NO_2^-, which was also used for NO_3^- absorption. The outflow of NO_2^- was with the fluid fraction from the rumen to the lower tract:

$$U_{NO_2^-;NO_2^-,Ex} = k_{Fl,Ex} \cdot Q_{NO_2^-} \quad (28)$$

and the reduction of NO_2^- to NH_3:

$$U_{NO_2^-;NO_2^-,NH_3} = k_{NO_2^-,NH_3} \cdot Q_{Mi} \cdot Q_{NO_2^-} \cdot Q_{H_2} \quad (29)$$

where $k_{NO_2^-,NH_3}$ denotes the rate constant for NO_2^- reduction to NH_3 by fermentative microbes (**Table 3**). The differential equation is given by:

$$\frac{dQ_{NO_2^-}}{dt} = P_{NO_2^-;NO_3^-,NO_2^-} - U_{NO_2^-;NO_2^-,Ab} - U_{NO_2^-;NO_2^-,Ex} - U_{NO_2^-;NO_2^-,NH_3} \quad (30)$$

Hydrogen state variable, Q_{H_2} [mol]. Influxes and outfluxes that were taken from Van Lingen et al. (2019) were the same as for the 3-NOP models and the reduced NO_3^- model. In the full NO_3^- model, output represented H_2 utilization for NO_3^- reduction to NO_2^- while applying a 1:1 stoichiometric ratio:

$$U_{H_2;NO_3^-,NO_2^-} = U_{NO_3^-;NO_3^-,NO_2^-} \quad (31)$$

and H_2 utilization for NO_2^- reduction to NH_3 while applying a 3:1 stoichiometric ratio:

$$U_{H_2;NO_2^-,NH_3} = 3 \cdot U_{NO_2^-;NO_2^-,NH_3} \quad (32)$$

Rumen methanogens without cytochromes were suggested to be inhibited by NO_2^- (Latham et al., 2016) at their electron-carrier system (Yang et al., 2016). Therefore, the flux that represented H_2 utilization for methanogenic growth that was incorporated accounted for inhibition by NO_2^-:

$$U_{H_2;H_2,CH_4} = \frac{\nu_{H_2,CH_4} \cdot Q_{Me}}{1 + \frac{M_{H_2;H_2,CH_4}}{C_{H_2}} + \frac{C_{NO_2^-}}{J_{NO_2^-;H_2,CH_4}}} \quad (33)$$

where $C_{NO_2^-}$ denotes the H_2 concentration, $J_{NO_2^-;H_2,CH_4}$ the inhibition constant for NO_2^- of the H_2 uptake rate for methanogenesis (**Table 3**). The differential equation is given by:

$$\frac{dQ_{H_2}}{dt} = P_{H_2;He,Ac} + P_{H_2;He,Bu} - U_{H_2;H_2,Me} - U_{H_2;NO_3^-,NO_2^-} - U_{H_2;NO_2^-,NH_3} - U_{H_2;H_2,Em} - U_{H_2;H_2,Ab} - U_{H_2;H_2,Ex.} \quad (34)$$

2.2. Model Input and Parameter Values

Inputs to the model were intake rate (shown in **Figures 1**, **2**) and nutrient composition of DM (**Table 4**). These inputs were taken from Van Zijderveld et al. (2011), Veneman et al. (2015), and Olijhoek et al. (2016) for the NO_3^- models, whereas the inputs were taken from Haisan et al. (2014), Hristov et al. (2015), Lopes et al. (2016), Haisan et al. (2017), and Van Wesemael et al. (2019) for the 3-NOP models. Every simulation was based on a dietary treatment with the inclusion rates of 3-NOP and NO_3^- that was supplemented. If the feed intake rate in time was not reported, feed intake rates were scaled to Olijhoek et al. (2016) for *ad libitum* feeding and scaled to Van Lingen et al. (2017) for restricted feeding. This scaling was done based on the fraction of daily feed intake consumed per hour of a day. The dietary nutrient contents and k_{FgHe} and k_{SgHe} for the different studies were set per dietary treatment and taken in accordance with Bannink et al. (2010) and CVB (2018). Non-identified fractions that may include pectin and fructan were assigned to Fg, Sg, and Wr as in Van Lingen et al. (2019). An overview of all nutrient contents and degradation characteristics is given in **Table 4**. For evaluating the biological significance of 3-NOP and NO_3^-

TABLE 4 | Degradable fiber (Fg), degradable starch (Sg), degradable protein (Pg) soluble sugars (Wr), acetate (Ac^-), propionate (Pr^-), butyrate (Bu^-), and lactate (La^-) feed contents [g·kg^{-1}], and fractional hydrolysis rates [h^{-1}] of degradable fiber and degradable starch per experiment and/or treatment assigned (ExpTr) for 3-NOP and NO_3^- model fitting data from Olijhoek et al. (2016, O), Van Zijderveld et al. (2011, VZ), Veneman et al. (2015, VM), Haisan et al. (2014, Hn1), Hristov et al. (2015, Hv), Haisan et al. (2017, Hn2), Lopes et al. (2016, Ls) and Van Wesemael et al. (2019, VW), and model evaluation data from Van Lingen et al. (2017, VL, average across all treatments and cows).

ExpTr	Fg	Sg	Wr	Ac^-	Pr^-	Bu^-	La^-	k_{FgHe}	k_{SgHe}	k_{PgPs}
Data for fitting NO_3^- models										
O	329	207	49	10	2	2	20	0.036	0.100	0.044
VZ	245	252	76	6	1	1	11	0.029	0.094	0.055
VM	294	230	90	13	2	2	26	0.025	0.100	0.054
Data for fitting 3-NOP models										
Hn1	281	250	140	0	0	0	0	0.056	0.091	0.067
Hv	198	244	157	3	0	0	5	0.043	0.087	0.070
Hn2	322	230	118	0	0	0	0	0.049	0.085	0.071
Ls	193	257	151	3	0	0	5	0.045	0.087	0.065
VW	315	149	116	6	1	1	12	0.042	0.081	0.053
Data for model evaluation										
VL	287	159	125	11	2	2	21	0.043	0.078	0.054

on the rumen microbial metabolism, the 3-NOP models were run for supplement inclusion rates of 0, 0.5, and 1.0 mmol·(kg DMI)$^{-1}$, whereas the NO_3^- models were run for inclusion rates of 0, 0.16, and 0.32 mol·(kg DMI)$^{-1}$. Dry matter intake rate and composition input data were from Van Lingen et al. (2017) on which various parameters of the extant model were fitted previously.

The differential equations of all state variables were numerically integrated for a given set of initial conditions and parameter values. The equations were solved using the lsoda numerical integration method (Petzold, 1983), a robust implicit integrator for stiff and non-stiff systems. This numerical integrator changes step size automatically to minimize computation time while maintaining calculation accuracy. The DM intake profile caused dramatic changes in Q_{H_2} shortly after feeding, which is why integration steps sizes were 2.5×10^{-3} h during the first 0.5 h and 10^{-2} h during the remaining hours of every consecutive 12 h period. Based on the absorption rate of NO_3^- and NO_2^- that was discussed to be slowly (Nolan et al., 2016), the $k_{NO_x^-,Ab}$ parameter was assigned a value of 0.30 h^{-1}, which is slightly lower than used for NH_3 and VFA absorption in the Dijkstra et al. (1996) model. Given the lack of data on 3-NOP absorption, the same value was used for the $k_{3NOP,Ab}$ parameter. Simulations based on the aforementioned collection of literature data were used for estimating the $J_{MCR;H_2,Me}$ and $k_{NO_3^-,NH_3}$ parameters of both 3-NOP models and the NO_3^- model to average daily CH_4 emission output. The $k_{NO_2^-,NH_3}$ and $J_{NO_2^-;H_2,Me}$ parameters of the NO_3^-+NO_2^- model were estimated to the diurnal H_2 and CH_4 emission rates that were extracted from the graphs presented in Van Zijderveld et al. (2011), Veneman et al. (2015) and Olijhoek et al. (2016). Including the k_{3NOP,NO_3^-}, k_{3NOP,NO_2^-}, and $k_{NO_3^-,NO_2^-}$ in the parameter estimation procedure resulted in limited identifiability and these three parameters were assigned values more arbitrarily, but such that NO_2^- concentrations in the 3-NOP+nitrite and nitrate+nitrate models approached the order of magnitude of the 3-NOP and NO_3^- concentrations, respectively.

To avoid numerical dispersion during the parameter estimation procedure and to correct for the model inaccuracy, the model was run using control treatment input (i.e., no supplementation of 3-NOP and NO_3^-) for every study, after which the observed CH_4 emission data for all dietary treatments for which a certain dose of 3-NOP and NO_3^- was administered were multiplied by the ratio of the observed and predicted values. A 240 h run of the model was considered to have converged to quasi steady-state. Model output of the final 24 h vs. the experimental data were calculated to assess the model performance given the model parameter values. The parameters were optimized to minimize the sum of squared residuals values using the BFGS algorithm (Conn et al., 1991).

2.3. Global Sensitivity Analysis

The sensitivity of the CH_4 emission rate to the parameters directly related to the inhibition was evaluated using a global sensitivity analysis. For this evaluation, the $J_{MCR;H_2,CH_4}$, $J_{NO_2^-;H_2,CH_4}$, $k_{NO_3^-,NO_2^-}$, $k_{NO_2^-,NH_3}$, k_{3NOP,NO_3^-}, k_{3NOP,NO_2^-}, $k_{NO_x^-,Ab}$, and $k_{3NOP,Ab}$ parameters of the 3-NOP+NO_2^- and NO_3^-+NO_2^- models drawn from 0.75 to 1.25 times their optimum value using Latin hypercube sampling and a sample size of 1.000. The sensitivity of CH_4 production was evaluated using the highest inclusion rates of 3-NOP and NO_3^- and the Van Lingen et al. (2017) feed input. Correlation coefficients were calculated to quantify the sensitivity of the CH_4 emission rate to the parameter values at 0, 0.5, 1, 2, 4, 6, and 10 h from the last meal of a 240 h simulation. All analyses were performed using the base

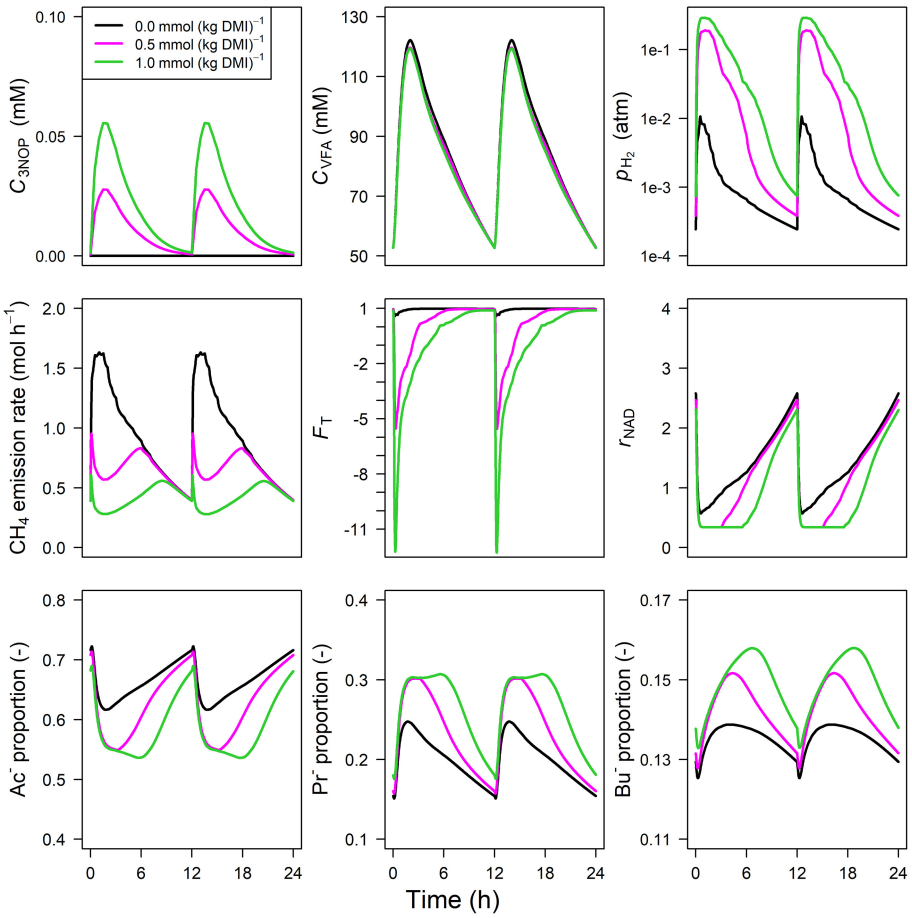

FIGURE 3 | Solutions of the 3-NOP dynamic model without NO_2^- representation [mM], VFA concentration [mM], rumen headspace p_{H_2} [atm], CH_4 emission rates [mol·h^{-1}], thermodynamic potential factor (F_T; [–]), NAD^+ to NADH ratio (r_{NAD}), acetate proportion (Ac^-), propionate proportion (Pr^-), and butyrate proportion (Bu^-).

(R Core Team, 2020) and FME packages (Soetaert and Petzoldt, 2010) in R statistical software.

3. RESULTS

3.1. Models Solutions

Parameter estimates of the optimized parameters of the four different models are provided in **Table 3**. In response to the assumed feed intake rate and all other parameters that were adopted from Van Lingen et al. (2019), all reference simulations in **Figures 3–6**, i.e., zero inclusion of 3-NOP and NO_3^-, are identical to the simulations shown in this study by definition. The present 3-NOP model predicts a 3-NOP concentration up to about 0.055 mM at 1.5 h from *in silico* feeding for the highest inclusion rate (**Figure 3**). Predicted 3-NOP concentrations then steadily approached zero at 12 h at which the next portion of feed was delivered. The diurnal dynamics of the total VFA concentration appeared largely unaffected by the inclusion of 3-NOP, whereas p_{H_2} clearly increased in response to 3-NOP inclusion, with a peak of 0.3 atm at about 1 h from feeding for the 1.0 mmol·kg^{-1} inclusion rate. The emission rate of H_2 followed a similar dynamic pattern as p_{H_2} (result not shown). In contrast to the increased peak in p_{H_2}, the CH_4 emission rate in response to 3-NOP decreased almost immediately after feeding and then increased to the reference emission rate, while C_{3NOP} approached zero. Increased p_{H_2} exerted increased thermodynamic inhibition of NADH oxidation, as indicated by the decreased minima of the thermodynamic potential factor (F_T; a dimensionless factor that corrects a predicted kinetic reaction rate for the thermodynamic control exerted; $F_T = 1$ indicates no thermodynamic inhibition; $F_T = 0$ indicates equilibrium between forward and reverse reaction or, in other words, complete inhibition of the chemical reaction) and the prolonged decrease of r_{NAD}. It should be noted that for both non-zero inclusion rates of 3-NOP, r_{NAD} starts reconditioning toward basal level at about 3 and 5 h from feeding when F_T is equal to zero ($F_T = 0$ indicates neither the forward nor the reverse reaction of NADH oxidation are thermodynamically feasible). The decrease in r_{NAD} after feeding was prolonged by 3-NOP supplementation that also resulted in decreased acetate, increase propionate and increased butyrate proportions that were prolonged. Extending the 3-NOP model to the 3-NOP+nitrite

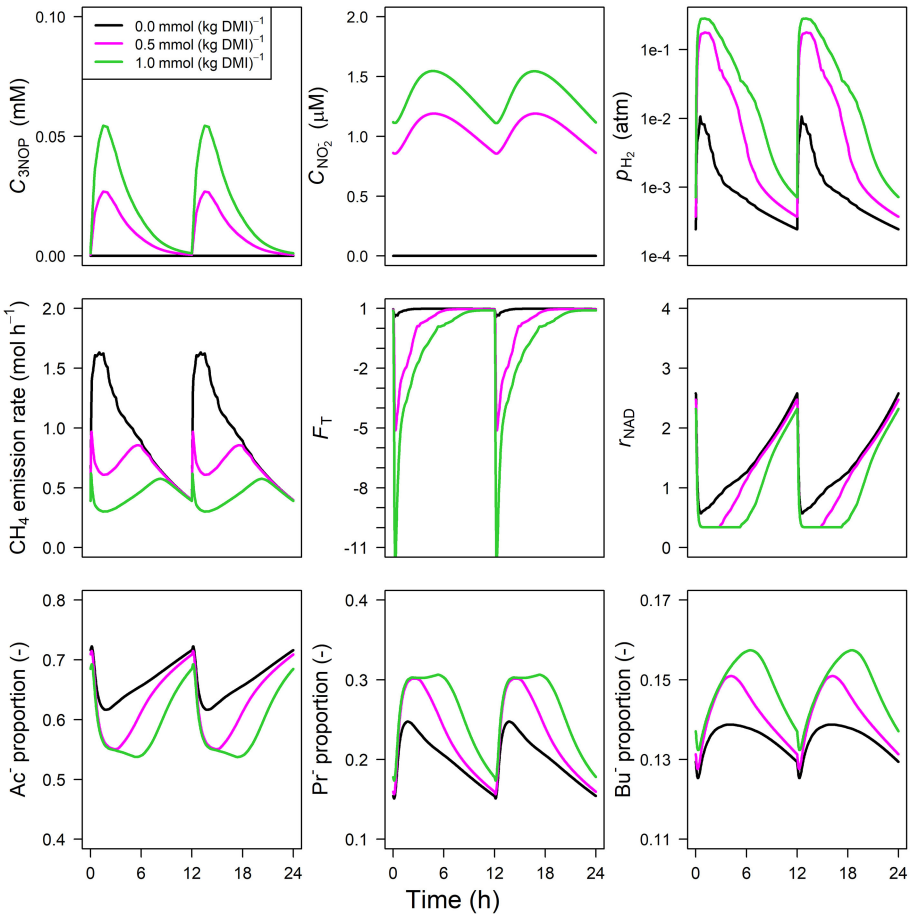

FIGURE 4 | Solutions of the 3-NOP dynamic model with NO_2^- representation for 3-NOP concentration [mM], NO_2^- concentration [μM], rumen headspace p_{H_2} [atm], CH_4 emission rates [mol·h^{-1}], thermodynamic potential factor (F_T; [–]), NAD^+ to NADH ratio (r_{NAD}), acetate proportion (Ac^-), propionate proportion (Pr^-), and butyrate proportion (Bu^-).

model had negligible effect on the dynamics of total VFA concentration (result not shown), whereas non-zero basal $C_{NO_2^-}$ and peaks of 0.2 and 0.5 μM at 3.25 and 2.75 h from feeding appeared for the two inclusion rates, respectively (**Figure 4**). Other dynamics predicted by the 3-NOP+nitrite model appeared similar to the 3-NOP model.

The concentration of NO_3^- predicted by the NO_3^- model showed an increase from 0 to 1.75 and 5.75 mM in 0.5 h for NO_3^- inclusion rates of 0.16 and 0.32 mol·kg^{-1} DMI, respectively, and then steadily approached zero at 12 h at which the next portion of feed was delivered (**Figure 5**). Peak p_{H_2} was clearly decreased and delayed in response to NO_3^- inclusion with a p_{H_2} value of 2.4×10^{-3} atm at 3.1 h from feeding for the 0.32 mol·kg^{-1} inclusion rate vs. 1×10^{-2} atm at 0.5 h for zero NO_3^- inclusion. A qualitatively similar decrease was simulated for the emission rate of H_2 (result not shown). In line with this decrease in H_2, the CH_4 emission rate was decreased compared to the reference simulation as well. Decreased p_{H_2} alleviated the thermodynamic inhibition of NADH oxidation, as indicated by F_T approaching one throughout almost the entire 24 h simulation period for the highest NO_3^- inclusion rate. The r_{NAD} and the proportions of acetate, propionate and butyrate were negligibly affected by the inclusion of NO_3^-, as was the total VFA concentration. Extending the nitrate model to the nitrate+nitrite model negligibly affected the dynamics of total VFA concentration (result not shown), whereas the $C_{NO_2^-}$ diurnal pattern qualitatively followed the $C_{NO_3^-}$ diurnal pattern (**Figure 6**). In contrast to the nitrate model, the nitrate+nitrite model predicted an increase in p_{H_2} with a peak of $\sim 2.5 \times 10^{-2}$ atm from 1 to 2 h from feeding in response to NO_3^- inclusion in the diet, whereas a relatively similar decrease in CH_4 emission rate was simulated. In line with the increase in p_{H_2}, r_{NAD} and the proportions of acetate, propionate and butyrate decreased, decreased, increased and increased, respectively. When zooming in on the highest inclusion rate of NO_3^- using the nitrate+nitrite model, 2% passes out from the rumen after reduction to NO_2^-, 3% is absorbed after reduction to NO_2^-, 13% passes out from the rumen to the lower gastrointestinal tract, 32% is absorbed, and 51% undergoes complete reduction to NH_3. These percentages indicate that 51% + 0.25×(3%+2%) = 52% of the potential of

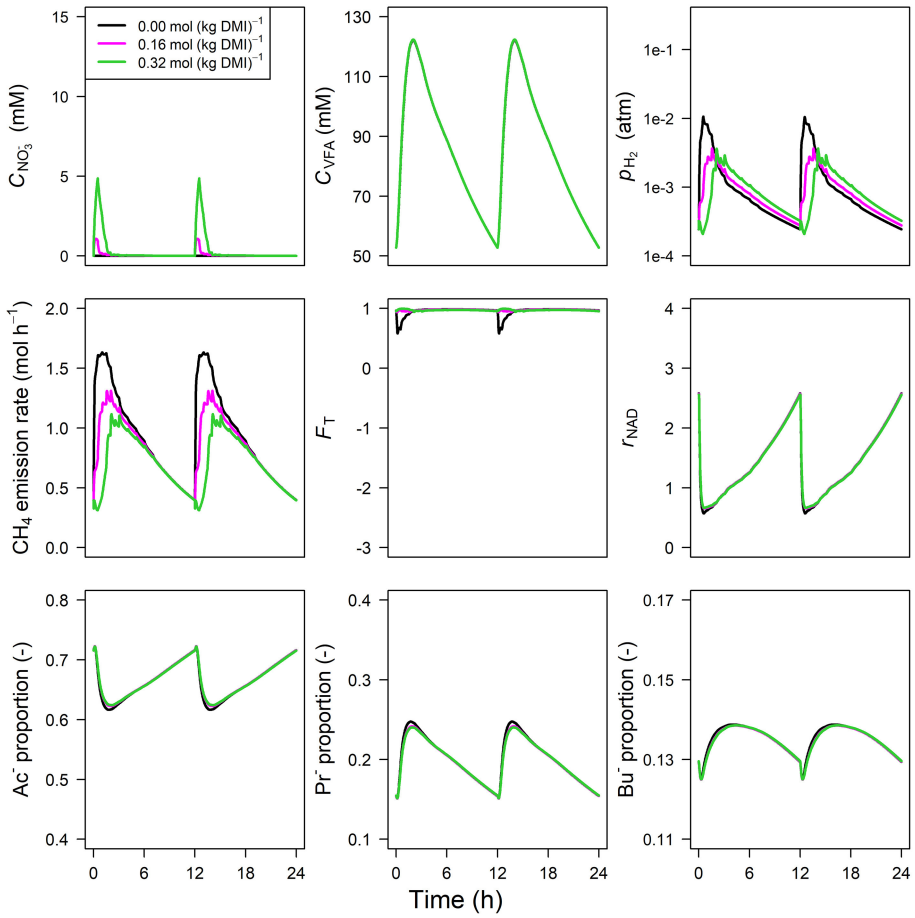

FIGURE 5 | Solutions of the NO_3^- dynamic model without NO_2^- representation for NO_3^- concentration [mM], VFA concentration [mM], rumen headspace p_{H_2} [atm], CH_4 emission rates [mol·h^{-1}], thermodynamic potential factor (F_T; [–]), NAD^+ to NADH ratio (r_{NAD}), acetate proportion (Ac^-), propionate proportion (Pr^-), and butyrate proportion (Bu^-).

NO_3^- as a H_2 sink is utilized, where 0.25 relates to one of the four H_2 equivalents for complete reduction of NO_3^- are consumed by fermentative microbes. Lastly, a qualitative overview of the output of the four different models in response to 3-NOP and NO_3^- supplementation is provided in **Table 1B**.

3.2. Global Sensitivity Analysis

The $J_{MCR;H_2,Me}$ inhibition parameter showed the strongest positive correlation with the CH_4 emission rate ($r = 0.6$ to 0.90) by the 3-NOP+nitrite model for the different time points for which the global sensitivity analysis was performed (**Figure 7**). The $k_{3NOP,Ab}$ parameter related to 3-NOP reduction also showed positive correlations, although the magnitude of the correlations was slightly stronger for the $J_{MCR;H_2,Me}$ parameter. The k_{3NOP,NO_2^-} absorption parameter was negligibly correlated to CH_4 emission rate at any of the time points. Correlations between the k_{3NOP,NO_3^-} parameter and CH_4 emission rate were also very minor, $|r| \leq 0.10$, but were consistently negative. For the nitrate+nitrite model, the $J_{NO_2^-;H_2,Me}$ inhibition parameter showed correlations of 0.61 to 0.97 from 0.5 to 6 h and correlations of approximately 0.5 at 0.0 and 10 h, whereas the $k_{NO_2^-,NH_3}$ parameter related to NO_2^- reduction showed the correlations from roughly 0.22 to 0.76 at the various time points. The $k_{NO_3^-,NO_2^-}$ parameter related to NO_3^- reduction showed very weakly negative correlations varying from −0.02 to −0.13. The $k_{NO_x^-,Ab}$ parameter related to absorption of NO_3^- and NO_2^- had the highest correlations of 0.78 and 0.57 at basal level, that is at 0 and 10 h, respectively, with the correlations at the other times points varying from 0.09 to 0.28.

4. DISCUSSION

The present paper presents models for simulating the dynamics of rumen metabolic physiology after supplementing two effective inhibitors of enteric CH_4 emissions from cattle, viz. 3-NOP and NO_3^-. It should be noted that 3-NOP is also economically profitable at farm level, whereas this could not be clearly indicated for NO_3^- (Alvarez-Hess et al., 2019). Furthermore, NO_3^- supplementation may increase the concentration of the NO_2^- intermediate to levels that are poisonous to the

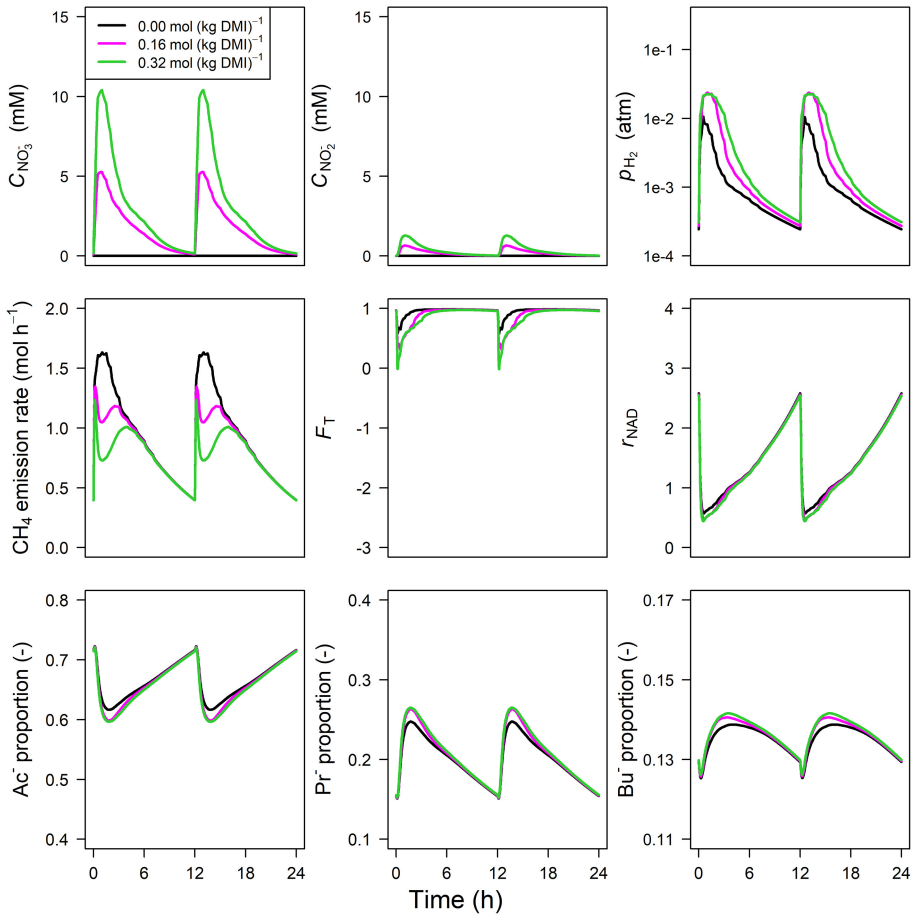

FIGURE 6 | Solutions of the NO_3^- dynamic model with NO_2^- representation for NO_3^- concentration [mM], NO_2^- concentration [mM], rumen headspace p_{H_2} [atm], CH_4 emission rates [mol·h^{-1}], thermodynamic potential factor (F_T; [–]), NAD^+ to NADH ratio (r_{NAD}), acetate proportion (Ac^-), propionate proportion (Pr^-), and butyrate proportion (Bu^-).

animal. To the authors' knowledge, the present study is the first effort that describes the metabolism of methanogenic inhibition in the rumen using dynamic mechanistic modeling. Presenting 3-NOP and NO_3^- models aids to distinguish the mode of action of decreased CH_4 caused by supplementation of 3-NOP and NO_3^- to diets of cattle and other domestic ruminants, and explores further metabolic implications of H_2 accumulation and its impact on VFA dynamics. The latter metabolic changes were most clearly indicated by the two 3-NOP models. The 3-NOP to NO_2^- conversion rate of the 3-NOP+nitrite model did not affect the inhibition potential of administered 3-NOP, whereas the 3-NOP to NO_3^- conversion rate appeared to alleviate methanogenic inhibition. The different metabolic dynamics of the two NO_3^- models point to the significance of the impact of NO_2^- as an inhibitor of methanogenic archaea, in addition to the metabolic steps that reduce NO_3^- to NH_3 and serve as H_2 sinks. The present modeling framework by which methanogenesis is inhibited by the concentration of an inhibitor (3-NOP models and nitrate+nitrite model) is possibly applicable to a wider variety of methanogenic inhibitors that are fed to various ruminant species.

4.1. Parameter Estimation Procedure

Data availability is an important determinant of model parameter identifiability (e.g., Brun et al., 2001). Data used for parameter estimation of the present models comprised average daily CH_4 emissions for both 3-NOP models and the nitrate model, whereas data describing diurnal dynamics of H_2 and CH_4 emission rates were used for the nitrate+nitrite model. It would be ideal, however, to obtain data that describes the diurnal dynamics of metabolites and also includes rumen 3-NOP, NO_3^- and NO_2^- concentrations. A dataset that comprises the concentrations of all these metabolites would increase the identifiability of the parameters, particularly of the nitrate+nitrite and 3-NOP+nitrite models for which the k_{3NOP,NO_3^-}, k_{3NOP,NO_2^-}, $k_{NO_3^-,NO_2^-}$ and $k_{NO_x^-,Ab}$ parameters were not estimated to data. Such data would likely also increase the accuracy of the simulated diurnal profiles of the various metabolites. Despite a relatively large variation of ruminal NO_3^- and NO_2^- concentrations across published studies

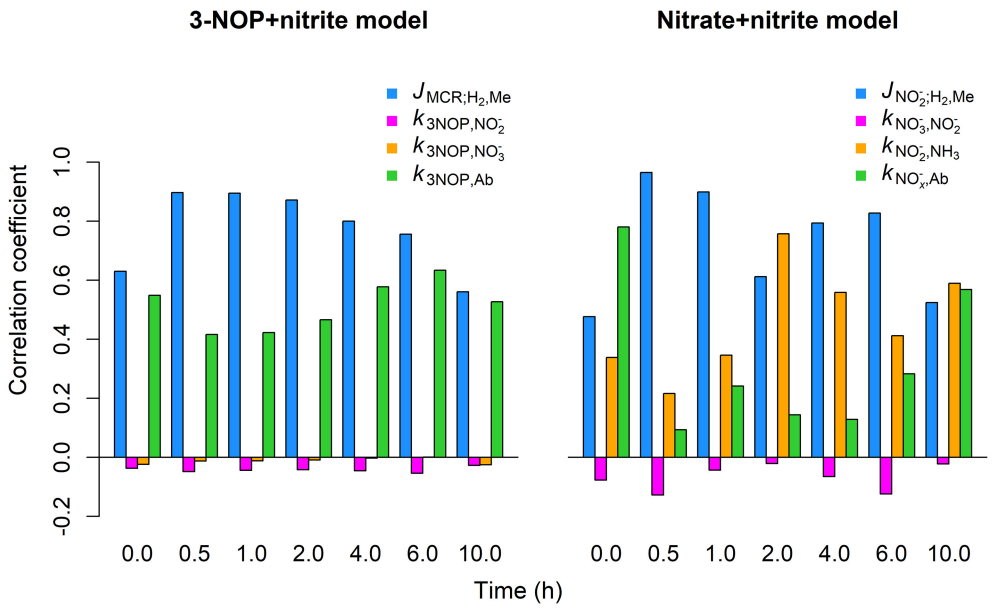

FIGURE 7 | Correlation between CH_4 emission rate and parameter values obtained from global sensitivity analysis for the 3-NOP+nitrite and nitrate+nitrite model when using inclusion rates of 1.0 mmol·kg^{-1} for 3-NOP and 0.32 mol·kg^{-1} for nitrate and the Van Lingen et al. (2017) feed input. Parameters values were drawn from the interval of 0.75 to 1.25 times their optimum value (see **Table 3**) using latin hypercube sampling and a sample size of 1,000. Correlation coefficents were calculated at 0, 0.5, 1, 2, 4, 6, and 10 h from the last meal of a 240 h simulation.

(e.g., Veneman et al., 2015; Wang et al., 2018), NO_3^- and NO_2^- concentrations of the same study were within the same order of magnitude for both studies. The NO_3^- and NO_2^- concentrations simulated using the nitrate+nitrite model are in the same order of magnitude as well, suggesting that our $k_{NO_3^-,NO_2^-}$ estimate has a fair degree of accuracy, given that the $k_{NO_2^-,NH_3}$ was highly identifiable to the diurnal profiles of H_2 and CH_4 emission. Although various parameters may not have the utmost accuracy, different estimates may not result in different conclusions being drawn regarding the mechanisms by which CH_4 production is inhibited and the sensitivity of the CH_4 emission rate to these parameters may not change and be more related to the overall developed model structures.

4.2. Inhibited Methanogenesis and Metabolism

The 3-NOP models predicted increased and decreased emission rates of H_2 and CH_4 upon 3-NOP supplementation, respectively, which indicated the model behavior was in line with various responses observed *in vivo* (e.g., Van Gastelen et al., 2020). The present models that are extensions of the Van Lingen et al. (2019) model, which accounts for the thermodynamic control of rumen fermentation by representing a H_2 pool and the inclusion of NAD^+ and NADH, predict thermodynamic inhibition of NADH oxidation and next more pronounced minima and maxima in VFA proportions after feeding 3-NOP supplemented feed. These predictions align with changes in VFA proportions that were observed *in vivo* (e.g., Haisan et al., 2014, 2017; Romero-Perez et al., 2015; Lopes et al., 2016). The similar responses of the 3-NOP and 3-NOP+nitrite models and the weakly negative correlation between the CH_4 emission rate and the k_{3NOP,NO_2^-} parameter obtained from the global sensitivity analysis indicate that the rate of NO_2^- production from 3-NOP has a minor effect on the inhibition of methanogenesis.

Extension of the nitrate model with a NO_2^- representation reversed the pattern of p_{H_2} and the H_2 emission rate in response to NO_3^- supplementation. The increased H_2 emission rate simulated using the nitrate+nitrite model reproduces the *in vivo* experiments used for model calibration (Van Zijderveld et al., 2011; Veneman et al., 2015; Olijhoek et al., 2016), and is also in line with increased dissolved H_2 concentration observed in faunated and defaunated *in vitro* systems (Wenner et al., 2020). This increase in dissolved concentration and emission rate of H_2 supports the role of NO_2^- as an inhibitor of methanogenesis (Iwamoto et al., 2002), which makes H_2 accumulate. The positive correlations observed from the global sensitivity analysis for the CH_4 emission rate with the $J_{NO_2^-;H_2,Me}$ and $k_{NO_2^-,NH_3}$ parameters point to the significance of the contribution of NO_2^- to the inhibition in CH_4 emission observed upon NO_3^- supplementation. The positive relationship between the $k_{NO_2^-,NH_3}$ parameter and the CH_4 emission rate suggests that the major mode of action of decreased CH_4 production after NO_3^- supplementation is caused by NO_2^- inhibition rather than H_2 that is consumed by the reduction of NO_2^- to NH_3. The very weakly negative correlations obtained for $k_{NO_3^-,NO_2^-}$ could be associated with decreased CH_4 emission by both H_2 sink reinforcement and NO_2^- accumulation resulting in inhibited methanogenesis, although the effect may be negligibly small based on the low

absolute correlations. If H_2 sink mechanisms were the key controller of the CH_4 emission rate, a negative relationship between the $k_{NO_2^-,NH_3}$ parameter and the CH_4 emission rate should have been obtained from the global sensitivity analysis, with increased reduction of NO_3^- and NO_2^- resulting in less CH_4. However, possibly in line with the low absolute correlations, Welty et al. (2019) only observed a numerical increase in dissolved H_2 concentration upon NO_3^- supplementation to a continuous culture and no increase in H_2 production. Therefore, the lack of H_2 accumulation in this specific study does not point to substantial methanogenic inhibition by NO_2^- in continuous cultures. Moreover, another possible explanation for unaffected H_2 concentration or production aligning with the present modeling study might be that their experimental conditions favored a rapid reduction of NO_2^- to NH_3 that alleviated the methanogenic inhibition by NO_2^-.

In line with Duin et al. (2016), the present 3-NOP+nitrite model also represents NO_3^- formation. Nitrate production from 3-NOP would alleviate the methanogenic inhibition as it does not block MCR, indicating that the proportion in which NO_3^- and NO_2^- are formed from 3-NOP may determine the persistence of the methanogenic inhibition of 3-NOP supplementation to cattle diets. However, the sensitivity analysis did not indicate the formation rates of NO_3^- and NO_2^- were substantially influential for the area of the parameters space that was explored. Lack of evidence for the presence of NO_3^- and NO_2^- reductases in rumen methanogens (Greening et al., 2019) may conceptually support the fact that NO_3^- formation alleviates methanogenic inhibition, because NO_3^- may then not be reduced to NO_2^-. However, Duin et al. (2016) observed 0.7 mol of NO_3^- and 0.2 mol of NO_2^- per mol of MCR when titrating with 3-NOP, which then requires one or more alternative mechanisms for the production of NO_3^- and NO_2^-. 1,3-propanediol also being formed from 3-NOP may suggest the production of NO_2 that is subsequently converted into NO_3^- and NO_2^-. The latter conversion has been described as a disproportionation reaction, which results in equimolar production of NO_3^- and NO_2^- (e.g., Park and Lee, 1988; Holleman and Wiberg, 2007). The production of 0.7 and 0.2 mol of NO_3^- and NO_2^-, respectively, may suggest either alternative NO_3^- production or NO_2^- utilization. If MCR deactivation by 3-NOP results in the formation of NO_2^- (Duin et al., 2016), MCR deactivation by NO_2^- may then result in the formation of NO (disproportionation also described by Park and Lee, 1988), which could explain why more NO_3^- than NO_2^- was observed. Furthermore, nitrate esters, which include 3-NOP, may hydrolyze and yield NO_3^- and an alkanediol (Baker and Easty, 1950, 1952). Although it is unknown if the latter hydrolysis reaction proceeds inside archaeal cells, it describes the production of NO_3^- and 1,3-propanediol from 3-NOP.

Nitrite at the outside or inside of archaeal cells will have consequences for the inhibition of archaeal physiology and methanogenesis. Whether or not transportation of NO_2^- across archaeal cell membranes takes place affects our understanding of methanogenic inhibition by NO_2^- derived from 3-NOP. Cabello et al. (2004) described some archaea, which are not abundant in the rumen, that possess NO_3^- transporters and NO_3^- and NO_2^- reductases. Therewith, these enzymes were not indicated in rumen methanogens. Furthermore, genes for nitrate and nitrite transporters were searched using the IGM/M online database (https://img.jgi.doe.gov/m/; Chen et al., 2019) using "Methanobrevibacter," "nitrate," "nitrite," and "transporter" did not point to any enzyme that possibly facilitates transportation of NO_2^- across the archaeal cell membrane, indicating that NO_2^- transportation across archaeal cell membranes is unlikely to occur. Nitrite inside archaeal cells, which is formed from 3-NOP that is transported across the archaeal cell membrane, contributes to blocking MCR and enhances methanogenic inhibition (Duin et al., 2016), although this specific study did not investigate if MCR inhibition is the only way in which NO_2^- inhibits CH_4 production. Besides MCR, membrane-associated enzyme complexes catalyze several metabolic steps of the methanogenic pathway in archaea without cytochromes (Thauer et al., 2008), which are the common methanogens in the rumen. Nitrite at the outside of archaeal cells may inhibit the membrane-associated enzyme complexes or disrupt the electron transport system of the membrane (Yang et al., 2016). In contrast to NO_3^- supplementation, 3-NOP supplementation results in substoichiometric ruminal concentrations of NO_2^-, which may indicate that the actual membrane-associated inhibition of methanogenesis is negligible based on the $J_{NO_2^-;H_2,Me}$ parameter for the NO_2^- model that is about two orders of magnitude greater than the $J_{MCR;H_2,Me}$ parameter for the two 3-NOP models. Furthermore, the value of the latter parameter could be taken as an additional indication for absence of NO_2^- transportation across archaeal cell membranes, because the methanogenic metabolism may be completely ceased by blocking of MCR if NO_2^- concentrations predicted after NO_3^- supplementation to cattle diets occur inside archaea. To the authors' knowledge, ceased methanogenic metabolism has not been observed upon ruminal NO_3^- supplementation, which may rule out that NO_2^- is transported into archaeal cells.

4.3. Hydrogen as a Controller of Fermentation

Inhibited methanogenesis resulted in increased p_{H_2} and H_2 emissions from the rumen, as simulated by both 3-NOP models using different inclusion rates as well as implementing methanogenic inhibition by NO_2^- when transitioning from the nitrate to the nitrate+nitrite model. Increased p_{H_2} exerted inhibition of NADH oxidation, which resulted in decreased proportions of acetate and increased proportions of propionate and butyrate (Van Lingen et al., 2016, 2019). These respective shifts in VFA proportions in response to p_{H_2}, which are also described by Janssen (2010), align with *in vivo* observations (Haisan et al., 2014, 2017; Lopes et al., 2016) for 3-NOP, whereas VFA proportions in response to NO_3^- supplementation seem less consistent in the literature. Observations were that acetate proportion was unaffected or increased, propionate proportion was unaffected, increased or decreased, and butyrate proportion was unaffected or increased across various studies (e.g., Guyader et al., 2015; Troy et al., 2015; Veneman et al., 2015; Olijhoek

et al., 2016; Wang et al., 2018). This somewhat diverse picture in response to NO_3^- may be related to the methanogenic inhibition that is likely employed, which is adverse to the H_2 sink mechanism in relation to thermodynamic inhibition of NADH oxidation and associated VFA proportions. Ruminal conditions that control the favorability of NO_2^- reduction may determine the occurrence of the H_2 sink mechanism and the methanogenic inhibition by NO_2^- mechanism. A mixed culture *in vitro* experiment by Anderson et al. (2016) indicated a decreased acetate to propionate ratio and an increased headspace p_{H_2} in response to increased NO_3^- supplementation, whereas these changes were impaired when the mixed culture was also inoculated with *Denitrobacterium detoxificans*, despite a more pronounced decrease of headspace CH_4 partial pressure. This inoculation may have stimulated the reduction of NO_2^- and alleviated methanogenic inhibition and H_2 accumulation, and next affected the production of the different VFA. Therefore, these observations will likely be reproduced by a nitrate model such as the present nitrate+nitrite model in which both the H_2 sink mechanism and the nitrite inhibition of methanogenesis mechanism are implemented.

Thermodynamic inhibition of NADH oxidation was greatest for the highest p_{H_2} that was simulated and changed VFA proportions the most, perhaps more than observed *in vivo*. Electron-bifurcating hydrogenases that are able of reoxidizing NADH oxidation (e.g., Buckel and Thauer, 2018), were found to be the primary mediators of H_2 production by a metatranscriptomics analysis, but this analysis did not indicate that these hydrogenases were expressed differently in high and low CH_4 emitting sheep (Greening et al., 2019). No differences between hydrogenase enzyme expressions in these two groups of sheep may not suggest that VFA proportions in ovine rumens were changed (Van Lingen et al., 2016) and also that the present modeling framework of rumen fermentation metabolism that did predict changes in VFA proportions is too simple. However, Greening et al. (2019) did not relate actual H_2 emissions to enzyme expressions, nor were their samples collected from animals that were fed diets known to induce inhibition of methanogenic archaea, which point to the need for future studies that explore these relationships. Nonetheless, the latter recent study did report evidence for differences in enzyme expression associated with various alternative H_2 utilizing pathways in high and low CH_4 emitting sheep. Besides decreased expression of methanogenic enzymes, they reported increased expression of enzymes that mediate fumarate reduction. Fumarate reduction produces succinate, which is a precursor of propionate. Therefore, increased fumarate reduction upon elevated p_{H_2} is expected to stimulate propionate production in the rumen, which qualitatively supports the present model predictions of increased propionate proportions upon feeding dietary substrate that induces methanogenic inhibition. Furthermore, a decrease in H_2 recovered as the sum of propionate, butyrate, H_2 and CH_4 was observed when inhibiting methanogenesis in both batch and continuous culture (Ungerfeld, 2015), although the specific energetic benefits of methanogenic inhibition depended on the type and concentration of the inhibitor and on the *in vitro* system.

A more exhaustive metabolic framework of ruminal H_2 dynamics may comprise more than the key mechanism by which hydrogenases produce H_2 and mediate NADH oxidation. Ungerfeld (2015) speculated that H_2 was incorporated in formate and microbial biomass, and perhaps taken away via reductive acetogenesis in continuous cultures. For the latter H_2 utilizing pathway, the p_{H_2} threshold may be as high as 2.5×10^{-3} atm (Poehlein et al., 2012). Administration of methanogenic inhibitors to the rumen increases the number of hours per day that this threshold is exceeded and may, therefore, stimulate reductive acetogenesis. Upon supplementating bromochloromethane as an methanogenic inhibitor to goats, a metagenomic analysis indicated that, apart from increased *Prevotella* and *Selenomonas* species that are able to produce propionate using the randomizing pathway, reductive acetogenic populations were also affected significantly suggesting that they provide minor contributions to the redirection of H_2 (Denman et al., 2015). In the previously cited metatranscriptomics analysis for sheep rumens (Greening et al., 2019), reductive acetogenesis was indicated and enzyme expression was negatively correlated to CH_4 yield. Therefore, the incorporation of the reductive acetogenic pathway in the present models may shed further light on the metabolic dynamics in the rumen upon supplementation of inhibitors. However, further studies are required to discover other so far unidentified H_2 sinks for a better understanding of the metabolic pathways involved in H_2 production and utilization (Guyader et al., 2017).

4.4. Summary of Main Findings

In conclusion, both 3-NOP models and the nitrate+nitrite model predicted that the H_2 emission rate and p_{H_2} increased with the inclusion rate of 3-NOP and NO_3^-, whereas a decreased CH_4 emission rate was simulated for these supplements. Omission of the NO_2^- state variable from the 3-NOP model did not qualitatively change the overall dynamics of H_2 and CH_4 emission and other metabolites. However, omitting the NO_2^- state variable from the NO_3^- model substantially changed the dynamics of H_2 and CH_4 emissions indicated by a decrease in the emission rates of these two gases after feeding. Increased p_{H_2} induced by methanogenic inhibition, after 3-NOP supplementation particularly, resulted in decreased proportions of acetate and increased proportions of propionate and butyrate, although the incorporation of alternative H_2 consuming pathways may contribute to less pronounced responses in VFA proportions being predicted. The findings of this modeling study provide deeper insights into the metabolic physiology of ruminal bacteria, protozoa and archaea in response to two effective inhibitors of enteric CH_4 production. These insights will contribute to a better use of antimethanogenic additives and therefore help reducing enteric CH_4 production and the total ecological footprint of ruminant livestock production in the future.

DATA AVAILABILITY STATEMENT

R code and data files that support the model simulations of this study can be found online at the GitHub

repository through: https://github.com/linge006/Modeling-inhibited-methanogenesis.

AUTHOR CONTRIBUTIONS

HL designed the research, performed all simulations of this study, and wrote the paper. HL, DY-R, and MK did the conceptualization. JF, EK, and MK supervised the work. EK and MK were responsible for the project administration. All authors reviewed drafts of the manuscript and approved the final version.

FUNDING

The research was funded by DSM Nutritional Products (Basel, Switzerland).

ACKNOWLEDGMENTS

Dana Olijhoek and Anne Louise F. Hellwing (Aarhus University, Denmark), Caroline Plugge (Wageningen University, The Netherlands), and Tim J. Hackmann (University of California, Davis, USA) are greatly acknowledged for helpful input and discussions.

REFERENCES

Alvarez-Hess, P. S., Little, S. M., Moate, P. J., Jacobs, J. L., Beauchemin, K. A., and Eckard, R. J. (2019). A partial life cycle assessment of the greenhouse gas mitigation potential of feeding 3-nitrooxypropanol and nitrate to cattle. *Agric. Syst*. 169, 14–23. doi: 10.1016/j.agsy.2018.11.008

Anderson, R. C., Ripley, L. H., Bowman, J. G. P., Callaway, T. R., Genovese, K. J., Beier, R. C., et al. (2016). Ruminal fermentation of anti-methanogenic nitrate-and nitro-containing forages *in vitro*. *Front. Vet. Sci*. 3:62. doi: 10.3389/fvets.2016.00062

Baker, J. W., and Easty, D. M. (1950). Hydrolysis of organic nitrates. *Nature* 166, 156–156. doi: 10.1038/166156a0

Baker, J. W., and Easty, D. M. (1952). Hydrolytic decomposition of esters of nitric acid. part I. general experimental techniques. alkaline hydrolysis and neutral solvolysis of methyl, ethyl, iso propyl, and tert.-butyl nitrates in aqueous alcohol. *J. Chem. Soc*. 77, 1193–1207. doi: 10.1039/jr9520001193

Bannink, A., Smits, M. C. J., Kebreab, E., Mills, J. A. N., Ellis, J. L., Klop, A., et al. (2010). Simulating the effects of grassland management and grass ensiling on methane emission from lactating cows. *J. Agric. Sci*. 148, 55–72. doi: 10.1017/S0021859609990499

Brun, R., Reichert, P., and Künsch, H. R. (2001). Practical identifiability analysis of large environmental simulation models. *Water Resour. Res*. 37, 1015–1030. doi: 10.1029/2000WR900350

Buckel, W., and Thauer, R. K. (2018). Flavin-based electron bifurcation, ferredoxin, flavodoxin, and anaerobic respiration with protons (Ech) or NAD^+ (Rnf) as electron acceptors: a historical review. *Front. Microbiol*. 9:401. doi: 10.3389/fmicb.2018.00401

Cabello, P., Roldan, M. D., and Moreno-Vivian, C. (2004). Nitrate reduction and the nitrogen cycle in archaea. *Microbiology* 150, 3527–3546. doi: 10.1099/mic.0.27303-0

Chen, I.-M. A., Chu, K., Palaniappan, K., Pillay, M., Ratner, A., Huang, J., et al. (2019). IMG/M v. 5.0: an integrated data management and comparative analysis system for microbial genomes and microbiomes. *Nucleic Acids Res*. 47, D666–D677. doi: 10.1093/nar/gky901

Conn, A. R., Gould, N. I. M., and Toint, P. L. (1991). Convergence of quasi-Newton matrices generated by the symmetric rank one update. *Math. Programm*. 50, 177–195. doi: 10.1007/BF01594934

CVB (2018). "Chemische samenstellingen en nutritionele waarden van voedermiddelen," in *CVB Veevoedertabel 2018*, eds J. W. Spek and M. C. Blok (The Hague: CVB Programma).

Denman, S. E., Martinez Fernandez, G., Shinkai, T., Mitsumori, M., and McSweeney, C. S. (2015). Metagenomic analysis of the rumen microbial community following inhibition of methane formation by a halogenated methane analog. *Front. Microbiol*. 6:1087. doi: 10.3389/fmicb.2015.01087

Dijkstra, J., Bannink, A., France, J., Kebreab, E., and van Gastelen, S. (2018). Antimethanogenic effects of 3-nitrooxypropanol depend on supplementation dose, dietary fiber content, and cattle type. *J. Dairy Sci*. 101, 9041–9047. doi: 10.3168/jds.2018-14456

Dijkstra, J., France, J., Neal, H. D. S. C., Assis, A. G., Aroeira, L. J. M., and Campos, O. F. (1996). Simulation of digestion in cattle fed sugarcane: model development. *J. Agric. Sci*. 127, 231–246. doi: 10.1017/S0021859600078011

Duin, E. C., Wagner, T., Shima, S., Prakash, D., Cronin, B., Yáñez-Ruiz, D. R., et al. (2016). Mode of action uncovered for the specific reduction of methane emissions from ruminants by the small molecule 3-nitrooxypropanol. *Proc. Natl. Acad. Sci. U.S.A*. 113, 6172–6177. doi: 10.1073/pnas.1600298113

Gerber, P. J., Steinfeld, H., Henderson, B., Mottet, A., Opio, C., Dijkman, J., et al. (2013). *Tackling Climate Change Through Livestock: A Global Assessment of Emissions and Mitigation Opportunities*. Food and Agriculture Organization of the United Nations (FAO), Rome.

Greening, C., Geier, R., Wang, C., Woods, L. C., Morales, S. E., McDonald, M. J., et al. (2019). Diverse hydrogen production and consumption pathways influence methane production in ruminants. *ISME J*. 13, 2617–2632. doi: 10.1038/s41396-019-0464-2

Guyader, J., Eugéne, M., Meunier, B., Doreau, M., Morgavi, D. P., Silberberg, M., et al. (2015). Additive methane-mitigating effect between linseed oil and nitrate fed to cattle. *J. Anim. Sci*. 93, 3564–3577. doi: 10.2527/jas.2014-8196

Guyader, J., Ungerfeld, E. M., and Beauchemin, K. A. (2017). Redirection of metabolic hydrogen by inhibiting methanogenesis in the rumen simulation technique (RUSITEC). *Front. Microbiol*. 8:393. doi: 10.3389/fmicb.2017.00393

Haisan, J., Sun, Y., Guan, L., Beauchemin, K. A., Iwaasa, A., Duval, S., et al. (2017). The effects of feeding 3-nitrooxypropanol at two doses on milk production, rumen fermentation, plasma metabolites, nutrient digestibility, and methane emissions in lactating Holstein cows. *Anim. Product. Sci*. 57, 282–289. doi: 10.1071/AN15219

Haisan, J., Sun, Y., Guan, L. L., Beauchemin, K. A., Iwaasa, A., Duval, S., et al. (2014). The effects of feeding 3-nitrooxypropanol on methane emissions and productivity of holstein cows in mid lactation. *J. Dairy Sci*. 97, 3110–3119. doi: 10.3168/jds.2013-7834

Holleman, A., and Wiberg, E. (2007). *Lehrbuch der Anorganischen Chemie, 102nd Edn*. Berlin: Walter de Gruyter GmbH Co KG. doi: 10.1515/9783110177701

Hristov, A. N., Oh, J., Giallongo, F., Frederick, T. W., Harper, M. T., Weeks, H. L., et al. (2015). An inhibitor persistently decreased enteric methane emission from dairy cows with no negative effect on milk production. *Proc. Natl. Acad. Sci. U.S.A*. 112, 10663–10668. doi: 10.1073/pnas.1504124112

Iwamoto, M., Asanuma, N., and Hino, T. (2002). Ability of *Selenomonas ruminantium*, *Veillonella parvula*, and *Wolinella succinogenes* to reduce nitrate and nitrite with special reference to the suppression of ruminal methanogenesis. *Anaerobe* 8, 209–215. doi: 10.1006/anae.2002.0428

Janssen, P. (2010). Influence of hydrogen on rumen methane formation and fermentation balances through microbial growth kinetics and fermentation thermodynamics. *Anim. Feed Sci. Technol*. 160, 1–22. doi: 10.1016/j.anifeedsci.2010.07.002

Kern, M., and Simon, J. (2009). Electron transport chains and bioenergetics of respiratory nitrogen metabolism in *Wolinella succinogenes* and other epsilonproteobacteria. *Biochim. Biophys. Acta* 1787, 646–656. doi: 10.1016/j.bbabio.2008.12.010

Latham, E. A., Anderson, R. C., Pinchak, W. E., and Nisbet, D. J. (2016). Insights on alterations to the rumen ecosystem by nitrate and nitrocompounds. *Front. Microbiol*. 7:228. doi: 10.3389/fmicb.2016.00228

Lopes, J. C., de Matos, L. F., Harper, M. T., Giallongo, F., Oh, J., Gruen, D., et al. (2016). Effect of 3-nitrooxypropanol on methane and hydrogen emissions,

methane isotopic signature, and ruminal fermentation in dairy cows. *J. Dairy Sci.* 99, 5335–5344. doi: 10.3168/jds.2015-10832

Nolan, J. V., Godwin, I. R., de Raphélis-Soissan, V., and Hegarty, R. S. (2016). Managing the rumen to limit the incidence and severity of nitrite poisoning in nitrate-supplemented ruminants. *Anim. Product. Sci.* 56, 1317–1329. doi: 10.1071/AN15324

Olijhoek, D. W., Hellwing, A. L. F., Brask, M., Weisbjerg, M. R., Højberg, O., Larsen, M. K., et al. (2016). Effect of dietary nitrate level on enteric methane production, hydrogen emission, rumen fermentation, and nutrient digestibility in dairy cows. *J. Dairy Sci.* 99, 6191–6205. doi: 10.3168/jds.2015-10691

Park, J., and Lee, Y. (1988). Solubility and decomposition kinetics of nitrous acid in aqueous solution. *J. Phys. Chem.* 92, 6294–6302. doi: 10.1021/j100333a025

Petzold, L. (1983). Automatic selection of methods for solving stiff and nonstiff systems of ordinary differential equations. *SIAM J. Sci. Stat. Comput*. 4, 136–148. doi: 10.1137/0904010

Poehlein, A., Schmidt, S., Kaster, A.-K., Goenrich, M., Vollmers, J., Thürmer, A., et al. (2012). An ancient pathway combining carbon dioxide fixation with the generation and utilization of a sodium ion gradient for atp synthesis. *PLoS ONE* 7:e33439. doi: 10.1371/journal.pone,.0033439

R Core Team (2020). *R: A Language and Environment for Statistical Computing*. Vienna: R Foundation for Statistical Computing.

Romero-Perez, A., Okine, E. K., McGinn, S. M., Guan, L. L., Oba, M., Duval, S. M., et al. (2015). Sustained reduction in methane production from long-term addition of 3-nitrooxypropanol to a beef cattle diet. *J. Anim. Sci.* 93, 1780–1791. doi: 10.2527/jas.2014-8726

Soetaert, K., and Petzoldt, T. (2010). Inverse modelling, sensitivity and Monte Carlo analysis in R using package FME. *J. Stat. Softw.* 33, 1–28. doi: 10.18637/jss.v033.i03

Thauer, R. K., Kaster, A.-K., Seedorf, H., Buckel, W., and Hedderich, R. (2008). Methanogenic archaea: ecologically relevant differences in energy conservation. *Nat. Rev. Microbiol.* 6:579. doi: 10.1038/nrmicro1931

Troy, S. M., Duthie, C. A., Hyslop, J. J., Roehe, R., Ross, D. W., Wallace, R. J., et al. (2015). Effectiveness of nitrate addition and increased oil content as methane mitigation strategies for beef cattle fed two contrasting basal diets. *J. Anim. Sci.* 93, 1815–1823. doi: 10.2527/jas.2014-8688

Ungerfeld, E. M. (2015). Shifts in metabolic hydrogen sinks in the methanogenesis-inhibited ruminal fermentation: a meta-analysis. *Front. Microbiol.* 6:37. doi: 10.3389/fmicb.2015.00538

Van Gastelen, S., Dijkstra, J., Binnendijk, G., Duval, S., Heck, J., Kindermann, M., et al. (2020). 3-nitrooxypropanol decreases methane emissions and increases hydrogen emissions of early lactation dairy cows, with associated changes in nutrient digestibility and energy metabolism. *J. Dairy Sci.* 103, 8074–8093. doi: 10.3168/jds.2019-17936

Van Lingen, H. J., Edwards, J. E., Vaidya, J. D., Van Gastelen, S., Saccenti, E., Van den Bogert, B., et al. (2017). Diurnal dynamics of gaseous and dissolved metabolites and microbiota composition in the bovine rumen. *Front. Microbiol.* 8:425. doi: 10.3389/fmicb.2017.00425

Van Lingen, H. J., Fadel, J. G., Moraes, L. E., Bannink, A., and Dijkstra, J. (2019). Bayesian mechanistic modeling of thermodynamically controlled volatile fatty acid, hydrogen and methane production in the bovine rumen. *J. Theoret. Biol.* 480, 150–165. doi: 10.1016/j.jtbi.2019.08.008

Van Lingen, H. J., Plugge, C. M., Fadel, J. G., Kebreab, E., Bannink, A., and Dijkstra, J. (2016). Thermodynamic driving force of hydrogen on rumen microbial metabolism: a theoretical investigation. *PLoS ONE* 11:e0161362. doi: 10.1371/journal.pone.0161362

Van Wesemael, D., Vandaele, L., Ampe, B., Cattrysse, H., Duval, S., Kindermann, M., et al. (2019). Reducing enteric methane emissions from dairy cattle: two ways to supplement 3-nitrooxypropanol. *J. Dairy Sci.* 102, 1780–1787. doi: 10.3168/jds.2018-14534

Van Zijderveld, S. M., Gerrits, W. J. J., Dijkstra, J., Newbold, J. R., Hulshof, R. B. A., and Perdok, H. B. (2011). Persistency of methane mitigation by dietary nitrate supplementation in dairy cows. *J. Dairy Sci.* 94, 4028–4038. doi: 10.3168/jds.2011-4236

Veneman, J. B., Muetzel, S., Hart, K. J., Faulkner, C. L., Moorby, J. M., Perdok, H. B., et al. (2015). Does dietary mitigation of enteric methane production affect rumen function and animal productivity in dairy cows? *PLoS ONE* 10:e0140282. doi: 10.1371/journal.pone.0140282

Wang, R., Wang, M., Ungerfeld, E. M., Zhang, X. M., Long, D. L., Mao, H. X., et al. (2018). Nitrate improves ammonia incorporation into rumen microbial protein in lactating dairy cows fed a low-protein diet. *J. Dairy Sci.* 101, 9789–9799. doi: 10.3168/jds.2018-14904

Welty, C. M., Wenner, B. A., Wagner, B. K., Roman-Garcia, Y., Plank, J. E., Meller, R. A., et al. (2019). Rumen microbial responses to supplemental nitrate II. Potential interactions with live yeast culture on the prokaryotic community and methanogenesis in continuous culture. *J. Dairy Sci.* 102, 2217–2231. doi: 10.3168/jds.2018-15826

Wenner, B., Wagner, B., St-Pierre, N., Yu, Z., and Firkins, J. (2020). Inhibition of methanogenesis by nitrate, with or without defaunation, in continuous culture. *J. Dairy Sci.* 103, 7124–7140. doi: 10.3168/jds.2020-18325

Yang, C., Rooke, J. A., Cabeza, I., and Wallace, R. J. (2016). Nitrate and inhibition of ruminal methanogenesis: microbial ecology, obstacles, and opportunities for lowering methane emissions from ruminant livestock. *Front. Microbiol.* 7:132. doi: 10.3389/fmicb.2016.0013

Conflict of Interest: MK is affiliated with DSM Nutritional products, which is the funder of the present study and patented 3-NOP.

The remaining authors declare that the research was conducted in the absence of any commercial or financial relationships that could be construed as a potential conflict of interest.

Publisher's Note: All claims expressed in this article are solely those of the authors and do not necessarily represent those of their affiliated organizations, or those of the publisher, the editors and the reviewers. Any product that may be evaluated in this article, or claim that may be made by its manufacturer, is not guaranteed or endorsed by the publisher.